Przybytkowski, Stanislaw Maciey

EFFECTS OF WALL INTERFERENCE ON UNSTEADY TRANSONIC FLOWS

The University of Arizona PH.D. 1983

EFFECTS OF WALL INTERFERENCE ON UNSTEADY TRANSONIC FLOWS

by

Stanislaw M. Przybytkowski

A Dissertation Submitted to the Faculty of the

PROGRAM IN APPLIED MATHEMATICS

In Partial Fulfillment of the Requirements
For the Degree of

DOCTOR OF PHILOSOPHY

In the Graduate College

THE UNIVERSITY OF ARIZONA

1 9 8 3

THE UNIVERSITY OF ARIZONA
GRADUATE COLLEGE

As members of the Final Examination Committee, we certify that we have read the dissertation prepared by Stanislaw M. Przybytkowski

entitled Effects of wall interference on unsteady transonic flows

and recommend that it be accepted as fulfilling the dissertation requirement for the Degree of Doctor of Philosophy.

C. Richard Suhan	May 2, 1983
	Date
W R Sears	May 2, 1983
	Date
F Ca[illegible]	May 2, 1983
	Date
Wilfred M. Greenlee	May 2, 1983
	Date
	Date

Final approval and acceptance of this dissertation is contingent upon the candidate's submission of the final copy of the dissertation to the Graduate College.

I hereby certify that I have read this dissertation prepared under my direction and recommend that it be accepted as fulfilling the dissertation requirement.

C. Richard Suhan	May 11, 1983
Dissertation Director	Date

STATEMENT BY AUTHOR

This dissertation has been submitted in partial fulfillment of requirements for an advanced degree at The University of Arizona and is deposited in the University Library to be made available to borrowers under rules of the Library.

Brief quotations from this dissertation are allowable without special permission, provided that accurate acknowledgment of source is made. Requests for permission for extended quotation from or reproduction of this manuscript in whole or in part may be granted by the head of the major department or the Dean of the Graduate College when in his judgment the proposed use of the material is in the interests of scholarship. In all other instances, however, permission must be obtained from the author.

SIGNED: 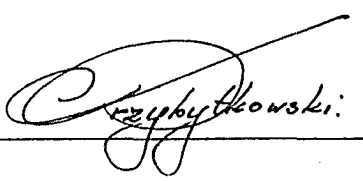

ACKNOWLEDGEMENTS

The author would like to express his deep gratitude and appreciation to Professor A.R. Seebass, Chairman of his committee, for his invaluable guidance and counsel during the course of this work. The author wishes also to thank the other members of his committee, especially to Dr. K.-Y. Fung for many helpful suggestions and stimulating discussions and to Professor W.R. Sears for his very helpful comments. Finally, Miss Linda Harper is thanked for her skillful typing of this dissertation

TABLE OF CONTENTS

LIST OF ILLUSTRATIONS

LIST OF ILLUSTRATIONS--continued

ABSTRACT

Various sources of error can cause discrepancies among flight test results, experimental measurements, and numerical predictions in the transonic regime. For unsteady flow, the effects of wind tunnel walls or a finite computational domain are the least understood and perhaps the most important. Although various techniques can be used in steady wind tunnel testing to minimize wall reflections, e.g., using slotted walls with ventilation, wind tunnel wall effects remain in unsteady wind tunnel testing even when they have been essentially eliminated from the steady flow. Even when the walls are ten chord lengths or more from the airfoil being tested, they can have a substantial effect on the unsteady aerodynamic response of the airfoil. In this study we compare numerical computations of two- and three-dimensional unsteady transonic flow with one another, and with experimental measurements, to isolate and examine the effects of tunnel walls.

An extension of the time-linearized code developed by Fung, Yu and Seebass (1978) is used to obtain numerical results in two dimensions for comparison with one another and with the experimental measurements of Davis and Malcolm (1980). The steady flow which is perturbed by small unsteady airfoil motions is found numerically by specifying the pressure distribution rather than the airfoil coordinates using the procedure provided by Fung and Chung (1982). This provides results that are nearly free from effects caused by the small

perturbation approximation; it also simulates the viscous effects present in the experimental measurements. A similar algorithm, developed especially for this study, is used for the related investigations in three dimensions. Different wall conditions are simulated numerically. Aside from a shift of frequency due to nonlinear effects, our numerical predictions of resonance conditions in two dimensions agree very well with those of linear acoustic theory.

A substantial discrepancy between unconfined computations and wind tunnel experiments is observed in the low frequency. This discrepancy highlights the importance of wall interference in wind tunnel measurements of unsteady transonic flow and delineates the conditions required to suppress them satisfactorily.

Chapter 1

INTRODUCTION

During the past decade there has been a large number of theoretical, numerical and experimental investigations of transonic flow phenomena aimed at the development of aircraft for flight at supercritical Mach numbers. The flight efficiency of turbojet powered aircraft is proportional to the Mach number until shock-waves appear and their effect on the boundary layer offsets the gains achieved by higher speeds. The development of supercritical wings in the early 1970's made flight at supercritical Mach numbers possible without the penalties associated with the presence of shock waves. Very special wing geometries have been developed that provide supersonic to subsonic recompression with only weak shock waves, or in some cases no shock wave at all.

Airplanes flying at all speeds have to be made relatively slender and, therefore, their wings are flexible and they may experience vibrations of an unstable nature. This phenomenon, called "flutter", is aeroelastic in nature, being driven by the interaction of the elastic forces of the structure of the aircraft wing with the unsteady aerodynamic forces generated by the oscillatory motion of the wing itself. Such vibrations, interacting with the passing airstream, may progressively increase their amplitudes by extracting energy from the flow and can even cause the disintegration of the wing structure

of the aircraft. There is normally a critical flight speed, the "flutter speed," for a given airplane wing structure above which flutter occurs. Because this phenomenon may have such serious consequences, the airplane flight speed must not reach or exceed its flutter speed. Since the vibration characteristics of the aircraft can be determined accurately by contemporary numerical methods or by ground vibration experiments, the accuracy of the flutter prediction is mainly determined by the accuracy with which the unsteady aerodynamic forces and moments can be predicted.

Because theoretical results are limited and numerical methods for the unsteady transonic flow about an arbitrary wing-body configuration are not yet fully developed, one usually relies on expensive wind tunnel experiments for the determination of flutter boundaries. Desirable testing conditions for an airplane would include an unconfined environment. Unfortuantely, most wind tunnel experiments are performed with the test section confined by walls or boundaries of some sort. Such walls have an effect on both steady and unsteady flow fields and, as we shall demonstrate, most especially on the unsteady aerodynamic response of the configuration.

There have been many attempts to eliminate or minimize wind tunnel wall interference. One notable method, proposed independently by Ferri and Baronti (1973) and by Sears (1974), is to use walls that are self-adaptive to minimize or eliminate the effects of the wind tunnel walls. The basic idea, in two dimensions for example, is to measure two flow-perturbation distributions (such as the velocity components

parallel and perpendicular to the free stream) away from the model and near the walls. Then, using only one such distribution as a boundary condition, the external flow field is computed. From this solution the second distribution is found. If this computed distribution is consistent with the measured one, then the tunnel is free of wall interference and accurately simulates unconfined flow. If this is not the case, there is wall interference and the walls have to be adjusted through changes in wall porosity, wall plenum pressure, etc., in order to reduce the difference between the measured distribution and the calculated one. This process is repeated until the flow is effectively free of wall interference. Thus, this process is an iterative one and it converges to unconfined steady flow conditions. For more information about convergence of this method the reader is referred to Sears (1977).

Another embodiment of the same principle, developed by Goodyer (1975) and others, is to use flexible wind tunnel walls so they can, through adjustment, align with a free stream surface. In this case one of the flow-perturbation distributions is just the slope of the wall and therefore only one such distribution has to be measured in the flow field. For example, one can measure the pressure distribution along a flexible wall.

Despite some advantages of the streamlined wall wind tunnel (for example, the possibility of simulating a cascade flow field), the first method seems to be better for unsteady disturbances because, while all the outgoing waves are reflected by a solid wall, they can

be absorbed to some extent by porous or slotted walls. The numerical experiments discussed in Chapter 4 indicate that low frequency disturbances are well absorbed at a slotted wall wind tunnel. This is not the case of higher reduced frequencies ($k \geq 0.2$).

Another way to simulate unsteady transonic flows is to develop theoretical models of such flows in which unconfined flow conditions can be easily simulated and solve them analytically or numerically. But simplifying assumptions must be made in order to have a computationally tractable problem. Thus, both these assumptions and the wall interference can be causes of discrepancies between numerical computations and experiments. The main goal of the present investigation is to isolate and delineate the effects of wind tunnel walls on unsteady two- and three-dimensional transonic flows.

Chapter 2

UNSTEADY TRANSONIC FLOWS

2.1 General Description of the Flow Field

Transonic flows over an airfoil are typically characterized by embedded supersonic regions terminated by nearly normal shock waves in an otherwise subsonic environment, as illustrated in Figure 1.

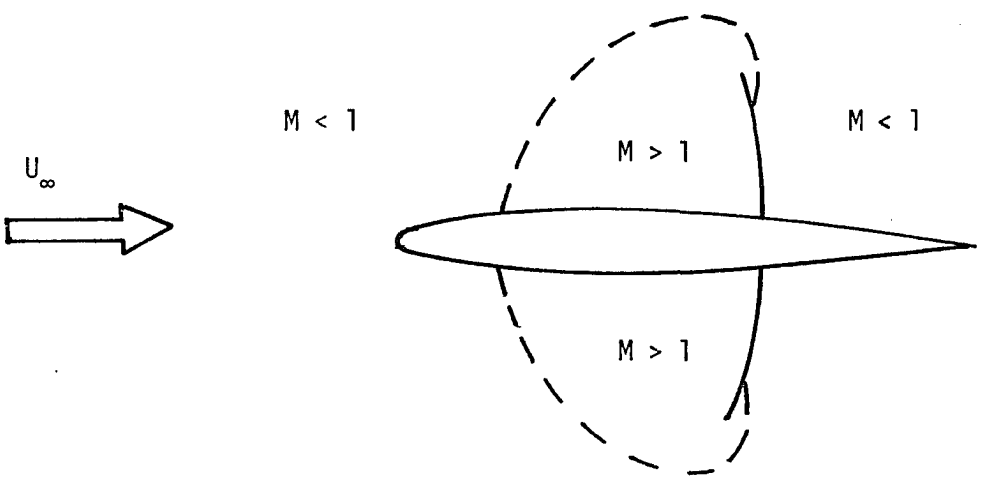

Figure 1. Schematic of steady transonic flow over a symmetrical airfoil.

This kind of flow pattern occurs when the free stream Mach number M is larger than the so-called critical Mach number M_{cr}. The critical Mach number is the free-stream Mach number for which the

maximum local Mach number in the flow is unity. When the free-stream Mach number increases, the shock moves aft and its strength and the size of the supersonic region both increase.

There are several viscous effects in the real flow including the boundary layer. The boundary layer is, of course, the thin viscous layer adjacent to the surface of a wing and in its wake, characterized by large normal gradients in the velocity which rise from zero at the surface to the local inviscid flow velocity at its outer edge. The presence of the boundary layer affects the pressure distribution on the wing and, therefore, its aerodynamic forces. The boundary layer flow near the airfoil surface due to viscous effects is retarded by the adverse pressure gradient induced by the shock wave over the rear portion of the airfoil. This thickens the boundary layer and affects the viscous separation at the trailing edge in a way that degrades the lift.

For cases of practical interest, the boundary layer, which starts at the leading edge, undergoes a transition from laminar to turbulent after a small fraction of the chord (5-10%). The magnitude of the boundary layer effect on the inviscid flow depends on the Reynolds number, which represents the ratio of enertial to viscous forces. The value of the Reynolds number determines the rate of growth of the boundary layer and the location of the transition point. If the shock is strong enough, it may cause the boundary layer to separate from the airfoil immediately after the shock or between the shock and the trailing edge. This interaction of the shock wave with the boundary layer can affect the entire inviscid flow field near the airfoil.

When the wing performs unsteady sinusoidal oscillations around a given axis, the circulation and, therefore, the local pressures and aerodynamic forces show periodic variations. According to Helmholtz's theorem, the total vorticity in the inviscid flow outside the boundary layer has to remain constant; hence, each time-dependent change in circulation around the airfoil generates free vorticity of the same strength but opposite sign at the trailing edge. This vorticity is carried downstream by the flow. The velocities induced by these free vortices around the wing change the instantaneous incidence of the wing in such a way that the oscillating part of the lift lags behind the motion of the wing.

Our goal is not the accurate numerical simulation of unsteady transonic flows, but rather the isolation and delineation of the effects of wind tunnel walls on the amplitude and phase of the forces and moments on both airfoils and wings. Thus, in this study, we confine ourselves to unsteady two- and three-dimensional inviscid and potential flows.

For small perturbation subsonic and supersonic flows, both the governing equation and the corresponding boundary conditions can be linearized. This means that the problem can be decomposed into the steady problem of flow about an airfoil and the unsteady problem of an infinitely thin flat plate oscillating in a uniform flow.

For transonic flows at low to moderate reduced frequencies, the governing equations can not be linearized because small nonlinear terms cause cummulative effects that become comparable to the linear

disturbances. This implies that the unsteady flow field can no longer be treated independently of the steady flow field. But from a practical point of view, there are advantages to some sort of linearization. A linearization about the nonlinear steady state is always possible if the amplitude of the unsteady part of the airfoils motion is small enough. But there is the question of whether or not the amplitudes of practical interest will be so small. Generally speaking, for the flutter investigations this is the case. For more details on this subject the reader is referred to the review paper by Tijdeman and Seebass (1980).

2.2 Governing Equations and Boundary Conditions

The complete equations describing the flow field are the Navier-Stokes equations. But even if we have at our disposal the latest computers such as the CRAY 1S or CYBER 205, these equations require more computational resources than are readily available for most problems of practical interest.

The first simplification that one can make for unsteady transonic flows is to assume that the flow is inviscid. This approximation is a good one because, for transonic flows of practical interest, the Reynolds number, Re, is large (typically 10^6 - 10^7) and viscous effects are confined to boundary layers and wakes that are thin. For laminar flow, for example, they would be $O(Re^{-1/2})$. If we assume the boundary layer remains attached over most of the wing, then the inviscid flow equations are a good approximation. The inviscid equations for

conservation of mass, momentum and energy give a system of five first-order partial differential equations with six unknowns. The system is completed by the equation of state. This system of equations, the Euler equations, is hyperbolic and quasilinear. Weak solutions to this hyperbolic system can be found numerically if the difference equations are derived from the conservative form of the equations. Because the structure of shock waves and the wake is governed by a balance between viscous and inertial terms, the difference schemes are usually constructed in such a way that the truncation error is of dissipative rather than dispersive character. In such calculations, the mesh size must be small in order that the length scale associated with the pseudo-viscosity of the truncation error be small compared to the length scale typical of the inviscid flow.

The Euler equations can be greatly simplified by assuming that the flow is irrotational. For the transonic flows of practical interest, the disturbance flow speeds in most of the flow field are small compared to the speed of sound. Additionally, the flow outside the boundary layer is and remains nearly irrotational. Vorticity is introduced by viscous effects in the boundary layers and shock waves. A consequence of Crocco's theorem is applied to weak shock waves that the vorticity behind the shock wave is proportional to the cube of the jump in the pressure across the shock wave. For the moderate strength shock waves that occur on the thin aircraft wings of practical interest, the irrotationality of the flow field is thus affected only to third order

in the disturbance size and the assumption of irrotational flow is consistent with, in fact better than, the small-disturbance approximation. For an irrotational flow, we can replace the velocity vector with the gradient of a scalar potential. This allows us to reduce the Euler equations to a single equation with one unknown, the velocity potential. And, because the flow disturbances are generally small, this equation can be markedly simplified.

Under the assumptions mentioned above, we now outline the derivation of the governing equations for our problem. A detailed derivation of the equations may be found in Landahl (1961).

As sketched in Figure 2, due to the presence of a thin body, the uniform flow of speed U_∞ is slightly perturbed.

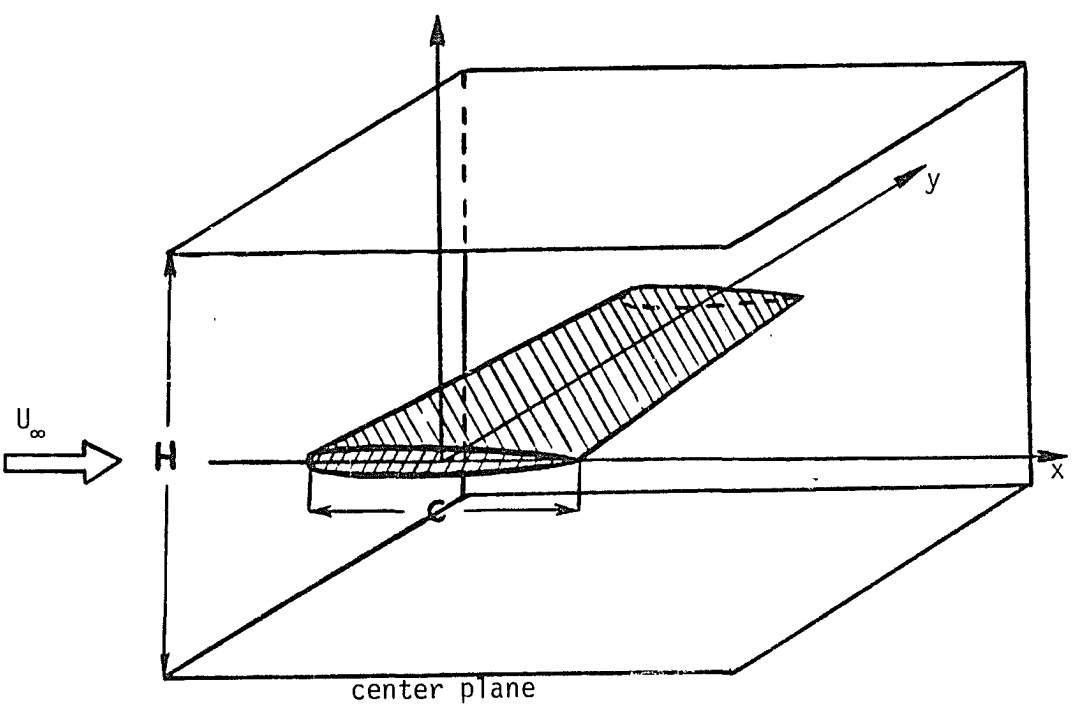

Figure 2. Sketch of a slender wing in a wind tunnel of height H showing the coordinate system used. The y = 0 plane is a plane of symmetry.

We introduce the non-dimensional small-disturbance velocity potential $\phi(x,y,z,t)$ such that the dimensional velocity components are

$$u = U_\infty(1 + \phi_x), \quad v = U_\infty \phi_y, \quad \text{and } w = U_\infty \phi_z \ ,$$

where U_∞ is the free stream velocity. Thus, derivatives of the potential are the size of the disturbance introduced by the wing. Here x, y and z are made dimensionless by dividing them by c, the chord of the wing at the root section, and t is made nondimensional by the characteristic time c/U_∞.

The conservation of mass requires that

$$\rho_t + [(1 + \phi_x)\rho]_x + (\rho\phi_y)_y + (\rho\phi_z)_z = 0 \tag{2.1}$$

where ρ denotes the density. In order to eliminate the derivatives of ρ, we may use the Bernoulli equation that follows from the momentum equation in the form

$$\phi_t + \phi_x + \frac{1}{2}(\phi_x^2 + \phi_y^2 + \phi_z^2) + \int \frac{dp}{\rho} = \frac{1}{M^2(\gamma-1)}$$

together with the equation of state for homentropic flow

$$p = \rho^\gamma \ .$$

Here γ is the ratio of specific heats and M is the local Mach number.

The differential equation governing small perturbations is the one which gives the correct first-order solution in the asymptotic sense when the perturbation velocities tend to zero. Therefore, assuming the disturbances are small and noncumulative terms can be

ignored, equation (2.1) can be simplified to the unsteady transonic equation first derived by Lin, Reissner and Tsien (1948), namely,

$$[(1 - M_\infty^2) - M_\infty^2(\gamma + 1)\,\phi_x]\,\phi_{xx} + \phi_{yy} + \phi_{zz}$$

$$= 2M_\infty^2\,\phi_{xt} + M_\infty^2\,\phi_{tt} \tag{2.2}$$

One of the advantages of using the small-disturbance equation for unsteady transonic flow is the simplicity of imposing boundary conditions on the wing. Assuming that our wing lies close to the $z = 0$ plane, and that the position of the wing at any instant of time can be defined by an equation $z = \tau F(x,y,t)$, where τ is the airfoil or wing thickness, we can express the first-order flow tangency condition as

$$\phi_z = \tau(F_x + F_t) \quad \text{on} \quad z^{\pm} = 0$$

and the pressure coefficient C_p on the wing, the quantity of most physical significance, is simply

$$C_p = -2(\phi_x + \phi_t) \quad \text{on} \quad z^{\pm} = 0,$$

where we recognize that the upper and lower surface of the wing now coincide with the plane $z = 0$.

To insure a unique solution within the inviscid approximation, we have to impose the Kutta condition that $[\![C_p]\!] = 0$ for the region behind the trailing edge of the wing. Here $[\![\ ]\!]$ denotes the jump across the wake behind the wing. At infinity, we require that the velocity perturbations vanish and that their integral around a large contour

be related to the circulation around the wing at an appropriate earlier time.

We should note here that the single quadratic term retained comes from the singular nature of the asymptotic expansion. Both $(1 - M_\infty^2)\ \phi_{xx}$ and $M_\infty^2(\gamma + 1)\ \phi_x\ \phi_{xx}$ are of second order in transonic flow where $(1 - M_\infty^2) = O(1)$. If one term is retained, the other must also be retained. Solutions to the equation that results from dropping these terms do not satisfy the far-field boundary conditions of decaying disturbances in much the same way that the solution $u(x,t) = \varepsilon f(x)$, which satisfies

$$u_t = 0,$$

with $u(x,0) = \varepsilon f(x)$, is an unsatisfactory approximation to the solution of

$$u_t + u\ u_x = 0$$

for small ε. That is, we must retain the $u\ u_x$ term because of its cummulative effect. We should note, however, that for unsteady motion of sufficiently high frequency, the derivative with respect to time on the right-hand side of equation (2.2) will be $O(1)$ and in this case it dominates the $\phi_x\ \phi_{xx}$ term hence this term can be dropped.

For harmonic oscillations of an airfoil or a wing we introduce the reduced frequency $k = \omega c/U_\infty$, where ω is the frequency of oscillation, and rewrite equation (2.2) as

$$[(1 - M_\infty^2) - M_\infty^2(\gamma + 1)\,\phi_x]\,\phi_{xx} + \phi_{yy} + \phi_{zz}$$

$$= 2M_\infty^2\, k\, \phi_{xt} + M_\infty^2\, k^2\, \phi_{tt} \,. \qquad (2.3)$$

Here we have replaced t by t'/k and then dropped the prime. This provides the correct scaling for the time derivatives; that is, their size is reflected now only in their coefficients.

The reduced frequencies of practical interest range from zero to O(1). At the larger reduced frequencies, amplitude effects are less important and a linearization, as noted above, provides the first approximation. At very low reduced frequencies, a quasi-steady approximation clearly holds. Thus, the reduced frequencies of principal interest are of order $\tau^{2/3}$. When $k = O(\tau^{2/3})$, we can clearly neglect the term $M_\infty^2\, k^2\, \phi_{tt}$ in equation (2.3). Thus, we have the well known equation for small-disturbance transonic flow at low reduced frequencies, namely,

$$2M_\infty^2\, k\, \phi_{xt} = [(1 - M_\infty^2) - M_\infty^2(\gamma + 1)\,\phi_x]\,\phi_{xx}$$

$$+ \phi_{yy} + \phi_{zz} \,. \qquad (2.4)$$

Although it is inconsistent with this approximation, we retain the term $k\, F_t$ in the boundary condition and the term $-2k\phi_t$ in the equation for the pressure coefficient C_p. This ad hoc approximation was first proposed by Houwink and van der Vooren in 1980. Retaining these terms provides better agreement between computations and experiments for the larber values of k. This can be understood by noting that their inclusion

correctly accounts for the finite speed with which the wake vorticity is transported downstream. Thus, the wake jump condition produces a circulation that is now a function of both time and space. Consequently, in this approximation vorticity travels downstream at nondimensional speed equal to 1/k. To be consistent, all O(k) terms except $k^2 \phi_{tt}$ are retained. Thus, the flow tangency condition is, with t scaled by 1/k,

$$\phi_z = \tau(F_x + k\, F_t). \tag{2.5}$$

Introducing the scaling transformations

$$a\,\tilde{\phi} = \phi, \quad \tilde{x} = x, \quad b\tilde{y} = y, \quad b\tilde{z} = z, \quad \text{and} \quad d\tilde{t} = t$$

where

$$a = \left(\frac{\tau^2}{(\gamma + 1)\, M_\infty^2} \right)^{1/3}, \quad b = (\tau(\gamma + 1)\, M_\infty^2)^{-1/3},$$

$$\text{and } d = 2M_\infty^2\, k\, b^2,$$

we find that equations (2.4) and (2.5) can be written as

$$\tilde{\phi}_{\tilde{x}\tilde{t}} = (\kappa - \tilde{\phi}_{\tilde{x}})\,\tilde{\phi}_{\tilde{x}\tilde{x}} + \tilde{\phi}_{\tilde{y}\tilde{y}} + \phi_{\tilde{z}\tilde{z}} \tag{2.6}$$

and

$$\tilde{\phi}_{\tilde{z}} = F_{\tilde{x}} + \frac{k}{d} F_{\tilde{t}} \tag{2.7}$$

where

$$\kappa = \frac{1 - M_\infty^2}{(\tau(1 + \gamma)\, M_\infty^2)^{2/3}} \quad \text{and} \quad \frac{k}{d} = \frac{1 - M_\infty^2}{2M_\infty^2\, æ} \ .$$

Here κ is the usual transonic similarity parameter and k is still an implicit parameter through the function F_t. We have stressed this by writing its coefficient as k/d although this coefficient is independent of k. Henceforth, we will use equations (2.6) and (2.7) but the tilda overbar ("~") will be dropped for simplicity.

For tutorial purposes, let us write the equation (2.6) in the simple form

$$-\phi_{xt} + \beta\phi_{xx} + \phi_{yy} + \phi_{zz} = 0 \ ,$$

where $\beta = \kappa - \phi_x$. Transforming variables by using $\eta = (1 - \beta)\, t - x$ and $\xi = (1 + \beta)\, t + x$, we have $-\phi_{\xi\xi} + \phi_{\eta\eta} + \phi_{yy} + \phi_{zz} = 0$.

Thus, equation (2.6) is hyperbolic for all values of β. It has been referred to erroneously as parabolic by Tijdeman and Seebass (1980) among others. Dropping the ϕ_{tt} term results in the instantaneous downstream propagation of disturbances, but two characteristics remain, as is clear from the above linear model: that for upstream-propagating waves and, as usual, the flow speed.

Chapter 3

NUMERICAL METHODS

3.1 Discretization of the Equations

Finite-difference methods have been popular in transonic flow computations since the success of Murman and Cole (1971) in treating mixed flows containing subsonic and supersonic regions using type-dependent differencing, which accounts for the fundamentally different, characteristics of subsonic and supersonic flows. However, it was shown by Jameson (1978) that their method allows stable expansion shocks which violate the entropy condition.

This difficulty was recently resolved by Engquist and Osher (1980), who introduced a monotone scheme for the small-disturbance transonic equation which does not allow the existence of stable expansion shocks. As demonstrated by Goorjian and Van Buskirk (1981) in their calculations of steady and unsteady transonic flow fields, this method also allows larger time steps for unsteady computations and has a faster convergence rate for steady computations than codes using a conservative Murman and Cole scheme. For the three-dimensional calculations presented here, we use standard finite-differences with the Murman and Cole type-dependent switching for subsonic and supersonic regions because of its simplicity and because it rarely produces expansion shocks.

As we have shown in the previous chapter, the governing equation is hyperbolic. Thus, one could use characteristics to calculate the flow field, but the Courant condition makes this far too slow. Thus, we elect to use an ADI scheme developed for parabolic equations because of its stability characteristics and its success in two dimensions. Nevertheless, one could also use an ADI scheme designed for hyperbolic equations, for example, the D'Yakonov's scheme [see, e.g., Mitchell (1976)], and this warrants further examination as it could lead to reduced computational effort.

3.2 Boundary Conditions

In order to study the effects of wind tunnel wall interference, we must calculate flows with and without wind tunnel walls. Thus, in our numerical model, we must provide for the boundary conditions on the wing, on the wind tunnel walls, and in the absence of such walls. Computational domains are always finite. To simulate unbounded conditions for a finite numerical domain, we may use, for example, an exponentially stretched grid so that the computational domain is mapped to a finite one. However, this stretching cannot be too severe or incident waves will effectively be reflected from grid spacing larger than themselves.

A better method, suggested by Fung (1981), is to prescribe asymptotic boundary conditions. If we assume that nonlinear effects (for example, shock waves) are confined to the neighborhood of the wing, the far-field potential of a vortex sheet of local strength $\Gamma(y,t)$ starting at the origin has the following form,

$$\phi = \frac{z}{y\pi} \int_{-AR/2}^{AR/2} \Delta\Gamma(\hat{y},t_o)\, g(x,y-\hat{y},z,t-t_o)\, d\hat{y} \qquad (3.1)$$

where $\Delta\Gamma$ is the circulation around the wing, AR is the aspect ratio (wing area/c^2) of the rectangular wings we consider here, and

$$g(x,y,z,t) = H[t + x - (x^2 + y^2 + x^2)^{1/2}]$$

$$\cdot[1 + x(x^2 + y^2 + z^2)^{-1/2}]/(y^2 + z^2)$$

Here H is the Heaviside function. This condition allows linear waves in phase with it to pass through without reflection. This boundary condition is derived using the low frequency approximation. For a motion starting at time t = 0, the low frequency approximation would insist that t_o = 0. Fung's implementation of the boundary condition assumes that it should be applied in the far-field at a t_o that corresponds to the time it takes a signal to propagate to the downstream boundary, and for him this is taken to be the order of Hk/c where H is large. The rational implementation of this condition in our case, where H is not large compared to the distance to the downstream boundary, is to consider the far-field due to a vortex sheet which travels downstream at a speed 1/k as important when its length is comparable to H. Thus, in our implementation, we have considered three t_o's:

$$t_o = n\,\frac{Hk}{c} \quad \text{where} \quad n = 0,\ 1,\ \text{and}\ 1.7\ .$$

The results are not especially sensitive to t_o in this range.

Another form of the boundary condition was proposed by Engquist and Majda (1981), namely,

$$\phi_n + \sqrt{\kappa^*}\,\phi_x = 0,$$

where ϕ_n is the normal derivative of the disturbance potential at the wall and $\kappa^* = \kappa - \phi_x$ for locally subsonic flow and $\kappa^* = \phi_x - \kappa$ for locally supersonic flow. This is a radiation boundary condition (it also models porous walls). The condition is deduced under the assumption that incident waves should be transmitted through the boundary. As we will see in the next chapter, this condition models the slotted wind tunnel wall for low-frequency unsteady oscillations quite well.

There have been some attempts to model mathematically the complicated conditions that apply at porous or slotted wind tunnel walls. The model for slotted walls developed by Bliss (1982) is one example, but no simple boundary condition can successfully model the complexity of a ventilated wind tunnel wall. This difficulty is easily understood when one realizes that in the flow close to the wind tunnel wall, viscous effects start to play an important role, and phenomena such as separation can occur when air is injected through the wall. We have chosen to use simple models of boundary conditions and use numerical experiments to determine which gives the best agreement with experiments.

The simplest boundary condition is the solid wall model given by

$$\phi_n = 0.$$

The boundary condition that models the porous wall can be written in the form

$$\phi_n + P\,\phi_x = 0,$$

where P denotes porosity. As one can see, by taking $P = \sqrt{\kappa^*}$ we recover the radiation boundary condition discussed earlier. Thus, one can model the porous wall by using the radiation boundary condition. For the slotted wall, one may write

$$\phi + A\,\phi_x = 0,$$

where A can be taken as a constant or a function. There is no clear interpretation of quantity A. The last two boundary conditions are ad hoc, and there is no convincing analytical argument that they should model either porous or slotted wall.

3.3 The Alternating Direction Implicit Method

The alternating direction implicit method introduced by Douglas and Rachford (1956) was used for the numerical discretization of the governing equations. This method splits one time step into three fractional steps in every space dimension - x, y and z.

The governing equation (2.6) for three dimensions expressed as an ADI scheme yields the following system of three equations:

$$\frac{\overleftarrow{\delta}_x(\phi^{n+1/3} - \phi^n)}{\Delta t} = \frac{1}{2}\,\delta_x^2(\phi^{n+1/3} + \phi^n) + \delta_y^2\,\phi^n + \delta_z^2\,\phi^n$$

$$\frac{\overleftarrow{\delta}_x(\phi^{n+2/3} - \phi^n)}{\Delta t} = \frac{1}{2}\,\delta_x^2(\phi^{n+1/3} + \phi^n) + \frac{1}{2}\,\delta_y^2(\phi^{n+2/3} + \phi^n) + \delta_z^2\,\phi^n \qquad (3.2)$$

$$\frac{\overleftarrow{\delta}_x(\phi^{n+1} - \phi^n)}{\Delta t} = \frac{1}{2}\,\delta_x^2(\phi^{n+1/3} + \phi^n) + \frac{1}{2}\,\delta_y^2(\phi^{n+2/3} + \phi^n) + \frac{1}{2}\,\delta_z^2(\phi^{n+1} + \phi^n)$$

where

$$\delta_x^2 = \begin{cases} (\kappa - \delta_{cx}\,\phi^n)\,\delta_{cx}^2 & \text{for the subsonic region} \\ 0 & \text{for the sonic line} \\ (\kappa - \overleftarrow{\delta}_x\,\phi^n)\,\overleftarrow{\delta}_x^2 & \text{for the supersonic region} \\ (\kappa - \delta_{cx}\,\phi_x^n)\,\delta_{cx}^2 + (\kappa - \overleftarrow{\delta}_x\,\phi_x^n)\,\overleftarrow{\delta}_x^2 & \text{across a shock wave.} \end{cases}$$

Here $\overleftarrow{\delta}_x$ is the first-order backward difference operator, $\overleftarrow{\delta}_x^2$ is the

second-order backward three-point difference operator, δ_{cx} is the first-order central-difference operator, and δ^2_{cx} is the second-order central difference operator, in the x direction. The subscripts y and z denote the corresponding second-order central-difference operators in the y and z directions.

Because all of these operators are linear, the system (3.2) can be written in a form more suitable for computations:

$$\left(\delta_x^2 - \frac{2\overleftarrow{\delta}_x}{\Delta t}\right)\phi^{n+1/3} = -\left(\delta_x^2 + 2\delta_y^2 + 2\delta_z^2 + \frac{2\overleftarrow{\delta}_x}{\Delta t}\right)\phi^n$$

$$\left(\delta_y^2 - \frac{2\overleftarrow{\delta}_x}{\Delta t}\right)\phi^{n+2/3} = \delta_y^2\,\phi^n - \frac{2\overleftarrow{\delta}_n}{\Delta t}\,\phi^{n+1/3} \qquad (3.3)$$

$$\left(\delta_z^2 - \frac{2\overleftarrow{\delta}_x}{\Delta t}\right)\phi^{n+1} = \delta_z^2\,\phi^n - \frac{2\overleftarrow{\delta}_x}{\Delta t}\,\phi^{n+2/3}$$

Because the operator δ_x^2 depends explicitly on values of the perturbation potential in the previous step, ^{n}, the scheme is first-order accurate in time and second-order accurate in space if the flow is subsonic. The operators $\overleftarrow{\delta}_x$ and δ_x^2 are either the central-difference operator or the backward-difference operators depending on whether the region on which they are applied is subsonic or supersonic. In the supersonic regions the spacial accuracy is first order. We use a quadra-diagonal matrix solver for the x-sweep and a tridiagonal solver for the y and z sweeps. For the case when the operator δ_x^2 does not depend on ϕ^n, for instance in the case of subsonic flow where δ_x^2 =

$\kappa\ \delta^2_{cx}$, one can show that this scheme is unconditionally stable. However, numerical experiments showed that this scheme is only conditionably stable for unsteady transonic flows. This instability is evidently caused by the moving shock waves. For stability, the time step must be small enough to insure that the shock wave moves less than one grid spacing.

The singularity at the leading edge that results from the small perturbation approximation could be another cause of difficulty and lead to instability. This could also be a source of instability for the codes such as LTRAN2 or LTRAN3. The LTRAN3 code, developed by Borland, Rizzetta and Yoshihara (1980) for calculating three-dimensional unsteady transonic flows over swept wings, retains certain cross derivative terms that are needed for swept wings. These lead to an additional time step limitation because they are treated explicitly rather than implicitly.

3.4 Time Linearization

The small-disturbance equation (2.6) can be linearized by assuming the unsteady flow field to be a small perturbation superimposed upon a given mean steady flow; in other words,

$$\phi(x,y,z,t) = \phi^0(x,y,z) + \varepsilon\psi(x,y,z,t) + O(\varepsilon)$$

where higher-order terms in ε are neglected. This restriction imposed on ε is dependent on the other parameters of the problem, i.e., κ and k.

Thus, we have from equations (2.6) and (2.7),

$$(\kappa - \phi_x^o)\,\phi_{xx}^o + \phi_{yy}^o + \phi_{zz}^o = 0,$$

with $\phi_z^o(x,y,0) = F_x^o(x,y)$ on the wing, and

$$\phi_{xt} = (\kappa - \phi_x^o)\,\psi_{xx} + \psi_{yy} + \psi_{zz}, \tag{3.4}$$

with $\psi_z(x,y,0,t) = F_x^u(x,y,t) + \frac{k}{d} F_t^u(x,y,t)$ on the wing, where $F(x,y,t) = F^o(x,y) + \varepsilon F^u(x,y,t)$. This approach was successfully applied by Ballhaus and Goorjian (1978) and by Fung, Yu and Seebass (1978). The steady flow field may be defined either by experimental or numerical means, providing an accurate description of the shock wave's geometry and strength.

Because of the ease of its practical implementation and the accuracy it achieves for small amplitude disturbances, time linearization is a very attractive method for calculating flutter boundaries. An additional advantage of time linearization is that it reduces the computational effort required because we can implement the indicial approach. That is, if the indicial response for an instantaneous change in some motion is known, then the solution for an arbitrary motion can be found with the aid of Duhamel's integral. Because of the indicial methods efficiency we used this method for our three-dimensional calculations of harmonic motions. For the indicial approach, we drop the $k\,F_t$ and $k\,\phi_t$ terms. This reduces its accuracy for the larger values of k considered.

Chapter 4

RESULTS AND DISCUSSION

4.1 Numerical Simulation of Wind Tunnel Wall Interference

In order to simulate unsteady transonic flows in a wind tunnel we use the different wind tunnel boundary conditions discussed earlier and, by numerical experiment, determine which of them gives the best agreement with experimental results. In the next two sections, our two-dimensional and three-dimensional numerical experiments are discussed.

As we shall see, this two-dimensional code models well the theoretical resonance conditions for solid wall boundary conditions, and the linear numerical results agree well with linear theory. For the three-dimensional cases, resonance also occurs and this phenomenon is captured by our numerical algorithm.

Our numerical experiments show that the boundary condition that best simulates slotted wall wind tunnels for low frequency airfoil or wing motions is the asymptotic boundary condition imposed at the wall location. This implies that the slotted wall can well absorb linear waves of low frequency and, for cases with such frequencies, the main cause of discrepancies in the phase lag between experimental measurements and computational results is flow field nonlinearities.

4.2 Two-Dimensional Numerical Experiments

For our two-dimensional numerical experiments, we use the time-linearized algorithm developed initially by Fung, Yu and Seebass (1978) and improved substantially by Fung (1981) and Fung and Chung (1982). This code will be referred to as UTFC, that is, unsteady transonic flow computation. Fung and Chung (1982) have shown that UTFC gives results that compare well with the fully nonlinear code LTRAN2-HI of Hessenius and Goorjian (1982) for the low and moderate frequencies of principal interest, but it is much more efficient than this fully nonlinear code. Moreover, the steady flow which is perturbed by small unsteady airfoil motions may be found numerically in UTFC by specifying an airfoil's pressure distribution rather than its coordinates. This provides results that are nearly free from the errors caused by the small perturbation approximation; it also simulates the viscous effects if one uses the experimentally determined steady state pressure.

For the two-dimensional study we did not use the indicial approach because of the efficiency of the UTFC code (about half a minute of CRAY-1S CPU time per cycle of harmonic motion). This compromises the results for the larger values of k.

We first examine unsteady transonic flow in a wind tunnel with solid walls, for which we have a limited thoeretical result. Because this result is for the fully linear case, we first set ϕ_x^0 equal to zero in the time-linearized code.

Comparisons of calculated unbounded flow and calculated fully linear flow with solid wall boundary condition are shown in Figure 3.

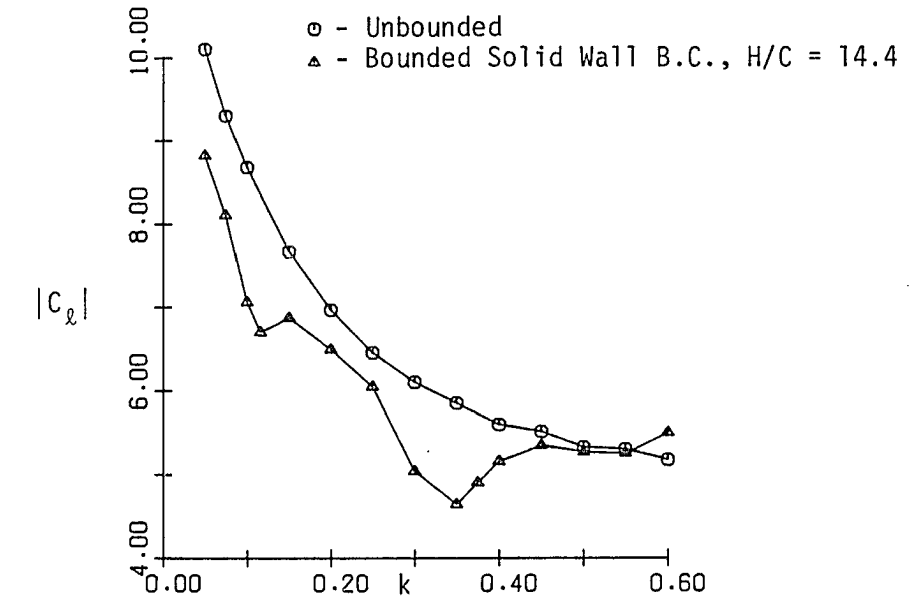

(a) Amplitude

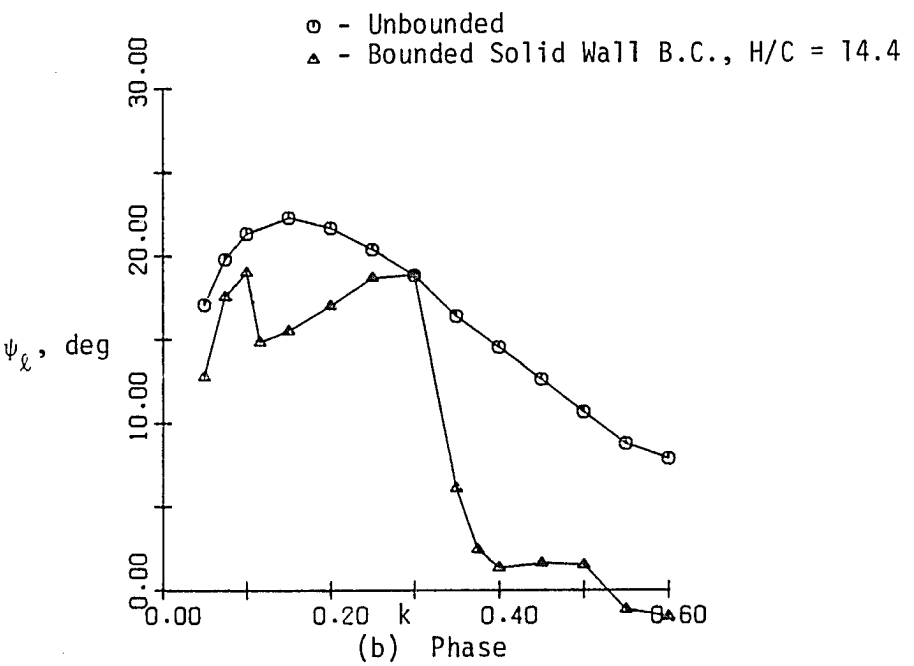

(b) Phase

Figure 3. Lift coefficients vs. reduced frequency for a pitching NACA 64A010 airfoil, $M_\infty = 0.8$, $C_\ell = \alpha_1 |C_\ell| \sin(\omega t - \psi_\ell)$, solid wall boundary conditions, linear calculations.

The wind tunnel height for the two-dimonsional solid wall case was 14.4 chord lengths. According to the linear theory of Woolston and Runyan (1955), the resonant frequencies for the solid-wall wind tunnel are given by the formula

$$k_r = \frac{c\pi}{HM_\infty} \sqrt{1 - M_\infty^2} \quad (2n - 1), \; n = 1, 2, 3, \ldots \qquad (4.1)$$

where k_r is the resonant reduced frequency, c is the chord length and H is the height of the wind tunnel. This condition is derived from the integral equation relating a known distribution of vertical velocity to an unknown distribution of lift, and involves a complicated kernel function. According to equation (4.1), we have resonance at two reduced frequencies, $k_{r1} = 0.162$ and $k_{r2} = 0.487$ for the free stream Mach number, $M_\infty = 0.8$. Our numerical linear experiments, calculated using a pitching NACA 64A010 airfoil, indicate two resonance frequencies, $k'_{r1} = 0.116$ and $k'_{r2} = 0.35$, as one can see in Figure 3(a).

Our results for the resonant frequencies are shifted towards lower frequencies from the theoretical results, but the ratio $k'_{r2}/k'_{r1} = 3.02$ is very close to that predicted by the linear theory, which is exactly three. This shift in frequencies is presumably caused by neglecting the term ϕ_{tt} in our computations. Nevertheless, the numerical results are in as good an agreement with the linear theory as can be expected.

Next we examine the same case but now we keep the ϕ_x^o term. This is the case of unsteady transonic flow with moving shocks. Comparisons of the unbounded flows, the experiments of Davis and Malcolm

(1980) carried out with slotted wind tunnel walls, and flows with solid wall boundary conditions, are shown in Figure 4. Our numerical experiments for a pitching NACA 64A010 airfoil again indicate two resonant frequencies, this time with $k'_{r1} = 0.125$ and $k'_{r2} = 0.325$, as shown in Figure 4(a). Aside from the shift in frequencies noted in the previous case, the ratio of k'_{r2} to k'_{r1} is 2.6 instead of 3. This close agreement between the linear theory and the numerical results is surprising in that the linear theory is not applicable to flows with shocks and supersonic regions. The nonlinear steady state results in resonant frequencies closer to one another and shifted towards lower frequencies. We note that again the resonant amplitude for the lowest frequency is smaller than that for the higher one.

It is easy to see from equation (4.1) that with $H \to \infty$ all resonant frequencies are shifted towards zero. But numerical experiments show that in addition to the frequency shift, the resonance is weaker when H grows and ultimately vanishes, as one would expect. For example, for H = 180 chord lengths, the curve for unbounded flows is the same independent of the boundary conditions used. The discrepancy in the phase lags should be noted; it will be discussed later.

We next examine non-reflective boundary conditions using the wall distance and free stream Mach number of the previous study. As we noted earlier, this boundary condition can also be interpreted as a porous wall boundary condition. Comparisons of the experimental results, numerical solutions calculated with the walls so far away from the airfoil that waves reflected from the computational boundaries do

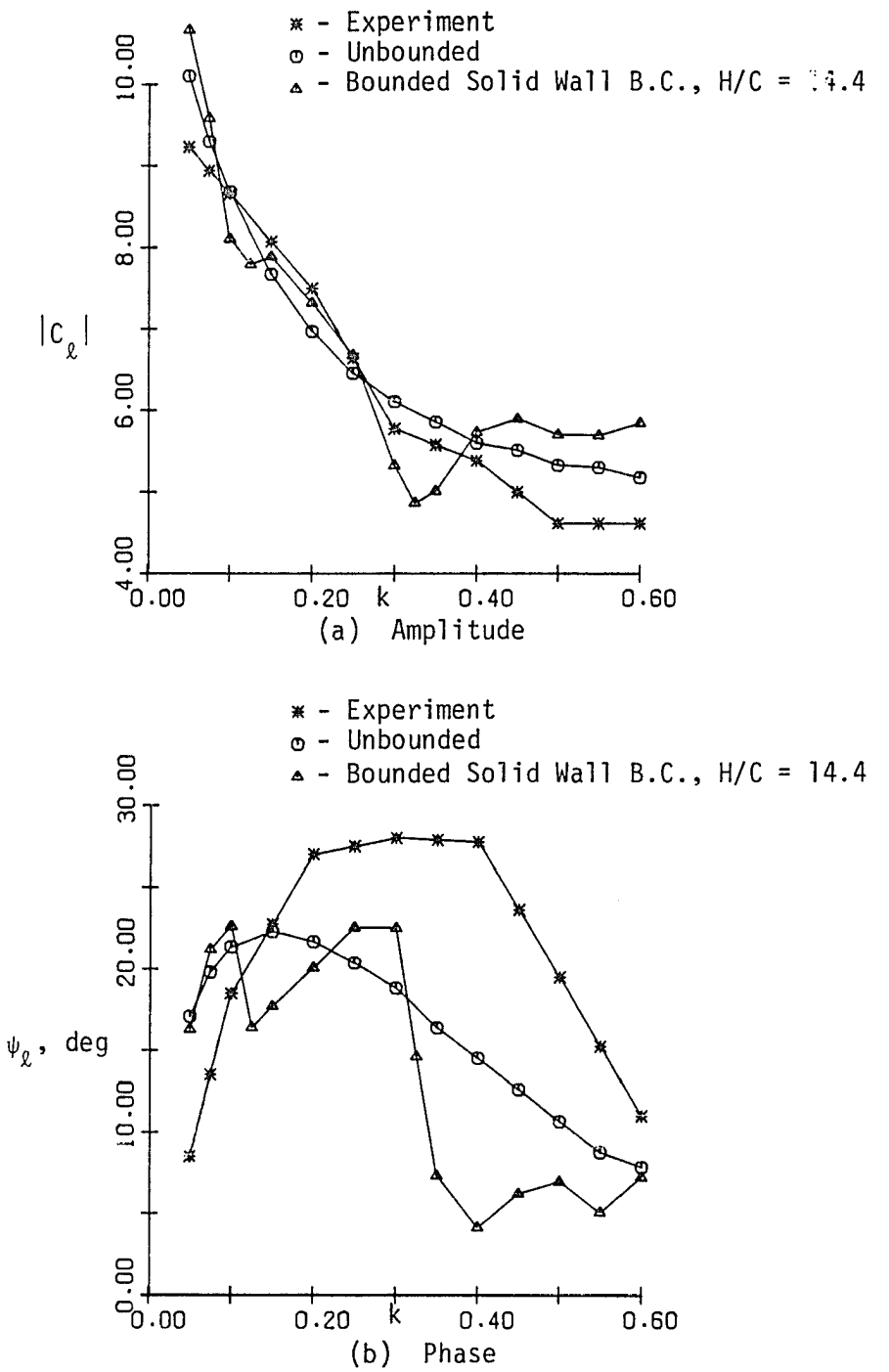

Figure 4. Lift coefficients vs. reduced frequency for a pitching NACA 64A010 airfoil, $M_\infty = 0.8$, $C_\ell = \alpha_1 |C_\ell| \sin(\omega t - \psi_\ell)$, solid wall boundary conditions.

not have time to return to the airfoil during the times of interest, and numerical experiments with walls are shown in Figure 5. The calculated amplitude with non-reflective boundary conditions follows very close to those of the experimental measurements for low frequencies, but they follow the unbounded computations for higher reduced frequencies. Thus, the discrepancies in phase lag between the experiment and the unconfined flow for $k \lesssim 0.2$ are due to nonlinear effects. That is, the slotted wind tunnel walls seem to cause experimental effects that are comparable to the nonlinear effects in the wave reflection process. Then nonlinear effects become less important as k increases, and this is evident in Figure 5.

We can see from this study that non-reflective boundary conditions give good agreement with those for unbounded flow even if they are imposed at a distance as small as 7.2 chord lengths from the airfoil. Since non-reflective boundary conditions give results similar to those obtained with the asymptotic boundary conditions at low reduced frequencies, and since the evaluation of boundary conditions is not the subject of the presented studies, we did not use these bound ary conditions in our three-dimensional numerical experiments.

The last numerical experiment in two-dimensions was performed with the same conditions as the previous study, except that the boundary conditions at the wall were replacec by the asymptotic expression

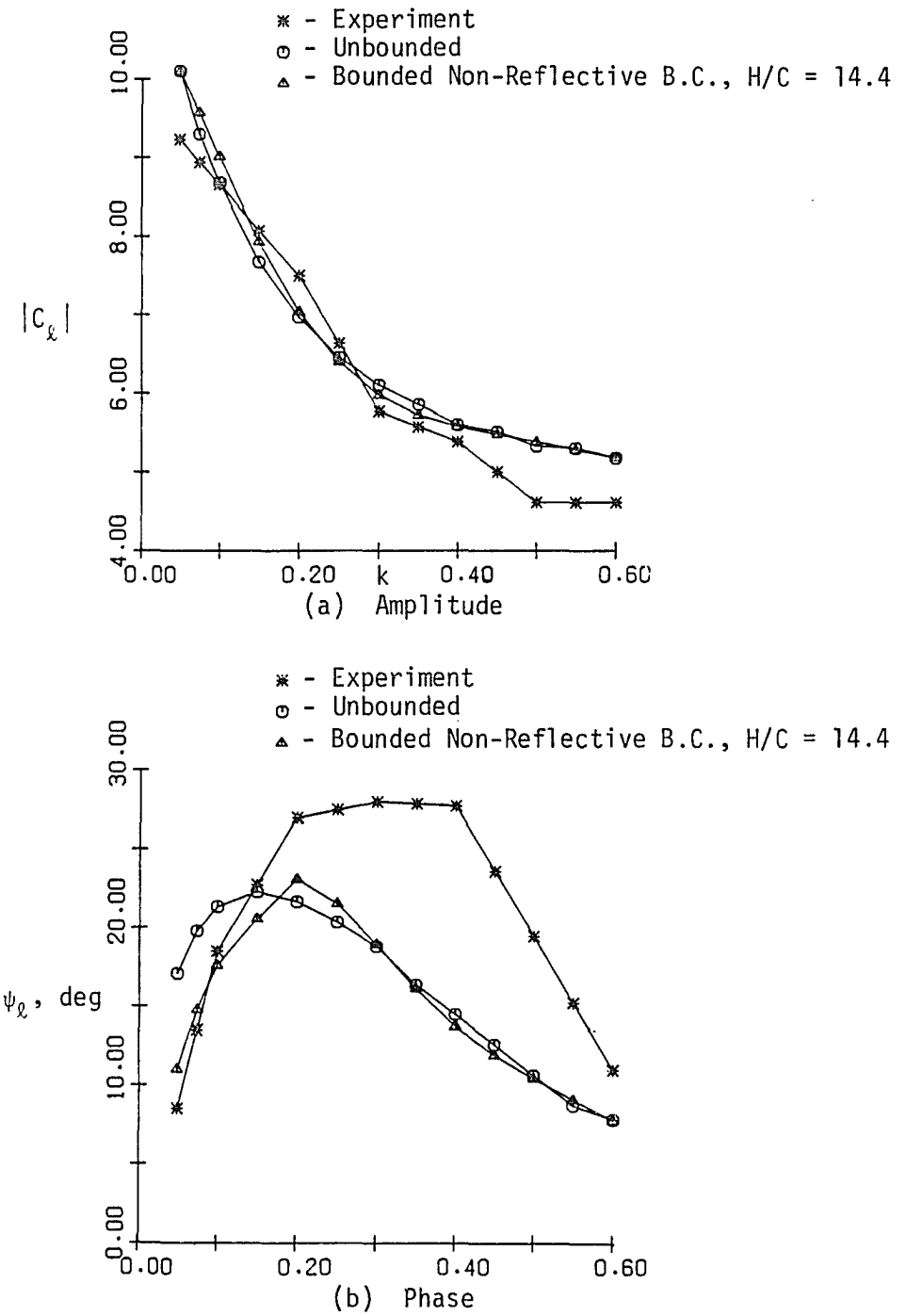

Figure 5. Lift coefficients vs. reduced frequency for a pitching NACA 64A010 airfoil, $M_\infty = 0.8$, $C_\ell = \alpha_1 |C_\ell| \sin(\omega t - \psi_\ell)$, non-reflective boundary conditions.

for the perturbation potential (3.1) discussed in Chapter 3. We note first by comparing Figures 5 and 6 that in general the non-reflecting boundary conditions are substantially better for modeling unconfined flow at the higher reduced frequencies. Comparisons of experimental results, numerical solutions for unbounded flow, and numerical experiments with walls simulated by expression (3.1) are shown in Figure 6. The amplitudes of the lift coefficient C_ℓ are almost the same for low reduced frequencies for all three cases (see Figure 6(a)). But the phase lags are quite different. The computed values follow the measured values of Davis and Malcolm (1980) almost esactly up to $k = 0.2$, but for higher reduced frequencies they depend on the choice of t_0, indicating the sensitivity of the phase lag to the wind tunnel wall conditions. The close agreement between the results for $n = 0$ and 1 stems from the fact that the results for those two integral values of n are in phase with one another. The result for $n = 1.7$ happens to agree very well with the experimentsl results, but this must be viewed as accidental. Again, we stress the sensitivity of the phase lag to t_0 and that serves to highlight the importance of avoiding wind tunnel wall reflection. As mentioned in Chapter 3, the asymptotic boundary condition allows linear waves to pass through without reflection at the numerical boundaries at low reduced frequencies where t_0 is appropriately zero. Thus, the discrepancies in phase lag between the non-reflecting and the asymptotic boundary conditions occur for $k \gtrsim 0.2$, as we would expect.

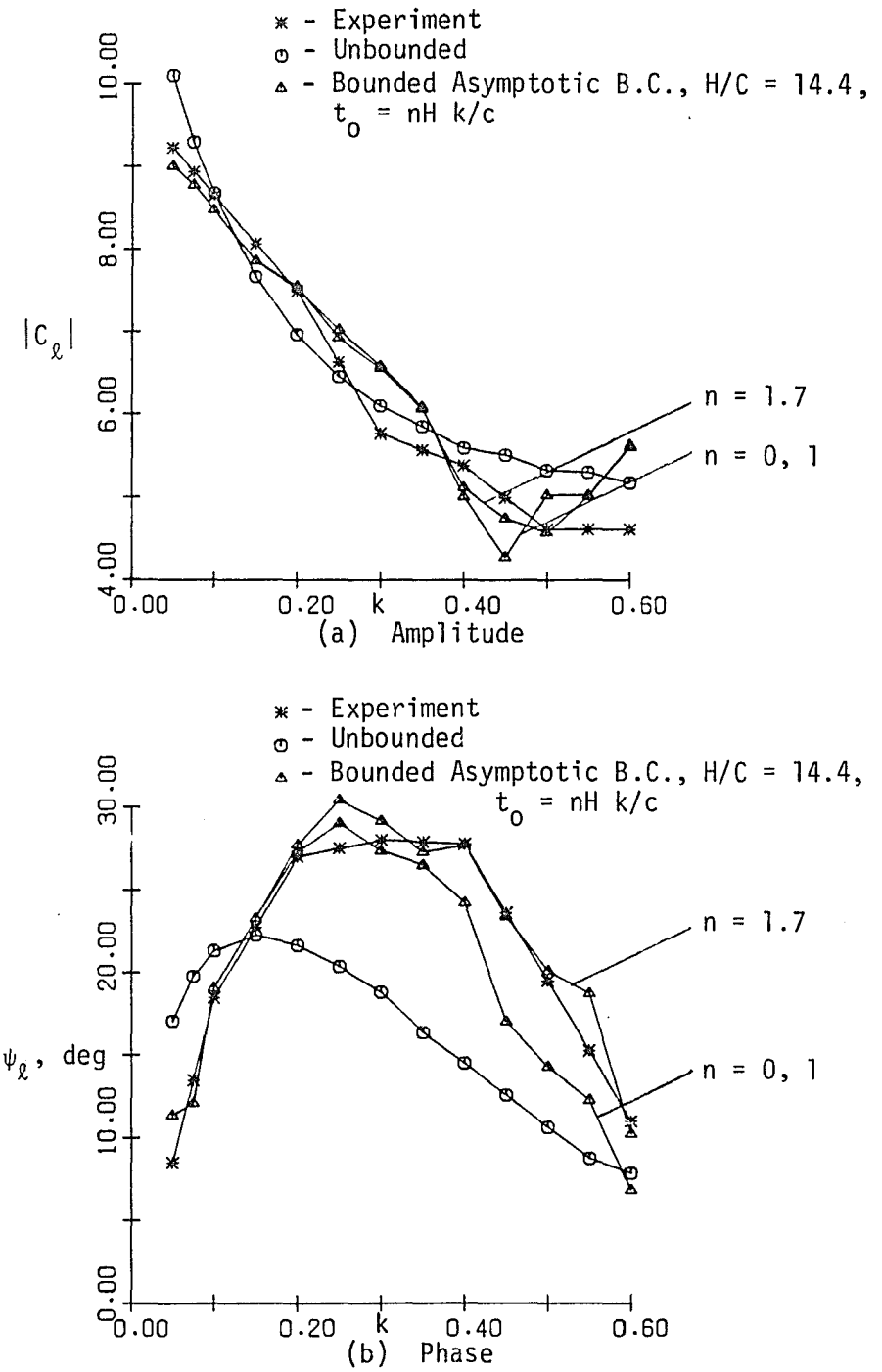

Figure 6. Lift coefficients vs. reduced frequency for a pitching NACA 64A010 airfoil, $M_\infty = 0.8$, $C_\ell = \alpha_1 |C_\ell| \sin(\omega t - \psi_\ell)$, asymptotic boundary conditions.

4.3 Three-Dimensional Numerical Experiments

The ADI algorithm that we discussed earlier was used to perform the three-dimensional numerical experiments analogous to those in Section 4.1 for two dimensions. The reader interested in the listing of the code and its description is referred to the report written by the author [Przybytkowski (1983)]. In the absence of corresponding three-dimensional unsteady experimental results, we compare the steady-state solution computed by the algorithm developed for this study with the three-dimensional computations of Bailey and Steger (1973) and with the two-dimensional experimental measurements of Davis and Malcolm (1980).

Figure 7 compares the calculated pressure distribution at the centerplane of a 6% thick parabolic-arc rectangular wing of aspect ratio 4.4 (span = 4.4 chords) with that from the computations of Bailey and Steger. Although the agreement is quite good, there are small discrepancies in the shock position and thickness. These are caused by application of non-conservative switching between supersonic and subsonic regions in the code of Bailey and Steger; as a consequence their scheme does not correctly capture the shock wave.

Comparison of our center plane results for steady flow with the two-dimensional experiment of Davis and Malcolm using the same airfoil section, an NACA 64A010, is provided in Figure 8. Here the agreement is also good, but again there is a difference in the shock thickness and position. Still, considering the fact that viscous effects result in a forward displacement of the shock wave, we must conclude that the numerical pressures agree very well with those measured experimentally.

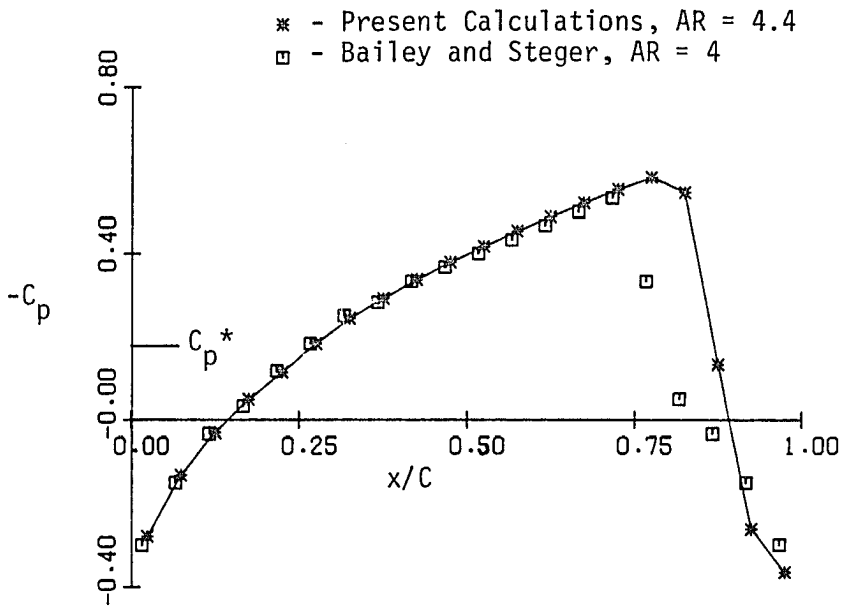

Figure 7. Pressure coefficient for a 6% thick parabolic-arc section at the root of a rectangular wing, M_∞ = 0.908, unbounded steady flow.

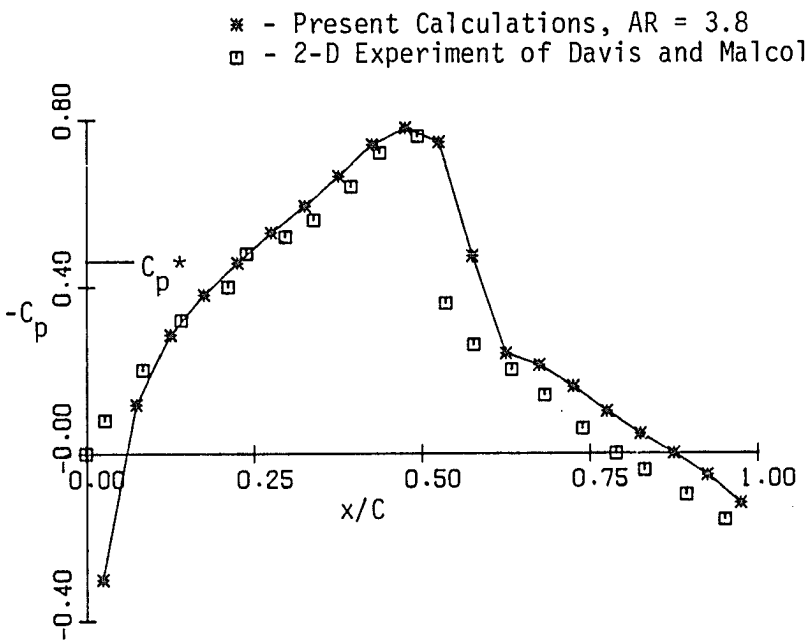

Figure 8. Pressure coefficient distribution for a NACA 64A010 section at the root of a rectangular wing, M_∞ = 0.9, unbounded steady flow.

Because of the high cost of unsteady three-dimensional calculations (about 10 minutes of CRAY-1S CPU time per cycle of harmonic motion), we use the indicial response of an input function. Thus, a sudden change in the incidence of the wing is used to obtain the corresponding results for harmonic motions of desired frequencies by application of the Duhamel's principle.

A comparison of unsteady three-dimensional computations with two-dimensional results is provided in Figure 9. The amplitudes of the lift coefficient for the three-dimensional case are generally below the two-dimensional values. This is a consequence of the fact that the pressure distribution is nearly two-dimensional at the center plane and the difference in pressure across the wing decreases towards the tip. Thus, the overall lift coefficient is smaller for three-dimensional flow than for two-dimensional flow. Note that the terms O(k) were dropped in these two-dimensional calculations to insure the comparison of results with the same approximations.

Next we consider unsteady three-dimensional flows in a wind tunnel with solid walls. Figures 10, 11 and 12 show the results for wind tunnels of square cross section of heights 8.5, 12.8 and 21.2 chord lengths respectively. In all three cases, the aspect ratio of the wing was AR = 3.8 (span = 3.8 chords). These three cases show qualitatively the same behavior as the analogous two-dimensional cases and the linear theory. We note that as H/AR increases from 2.23 to 5.58, the resonant frequencies decrease as the height of the wind tunnel increases and, at the same time, the resonant amplitudes become

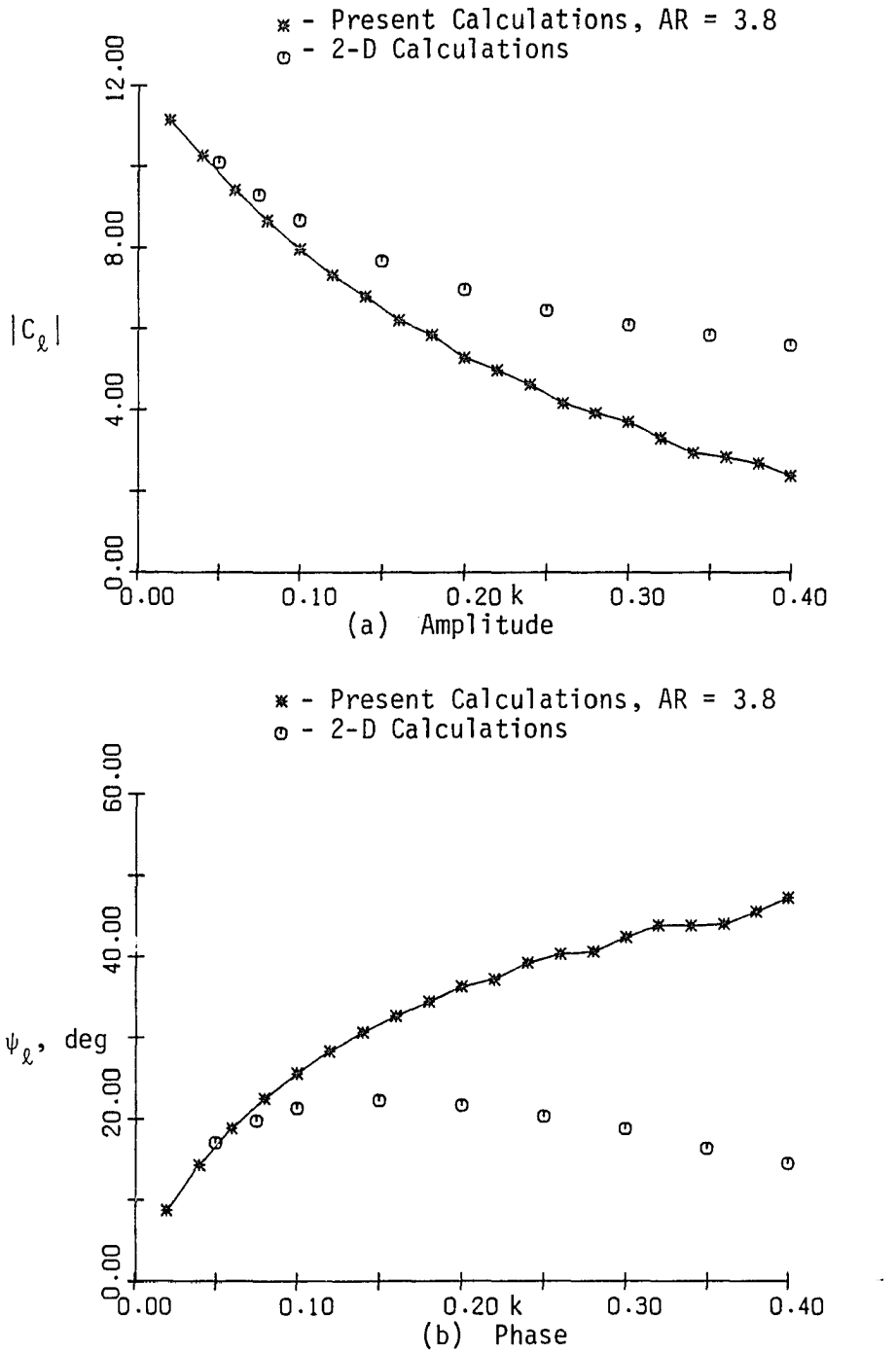

Figure 9. Lift coefficients vs. reduced frequency for a pitching NACA 64A010 airfoil, $M_\infty = 0.8$, $C_\ell = \alpha_1 |C_\ell| \sin(\omega t - \psi_\ell)$, unbounded flow conditions.

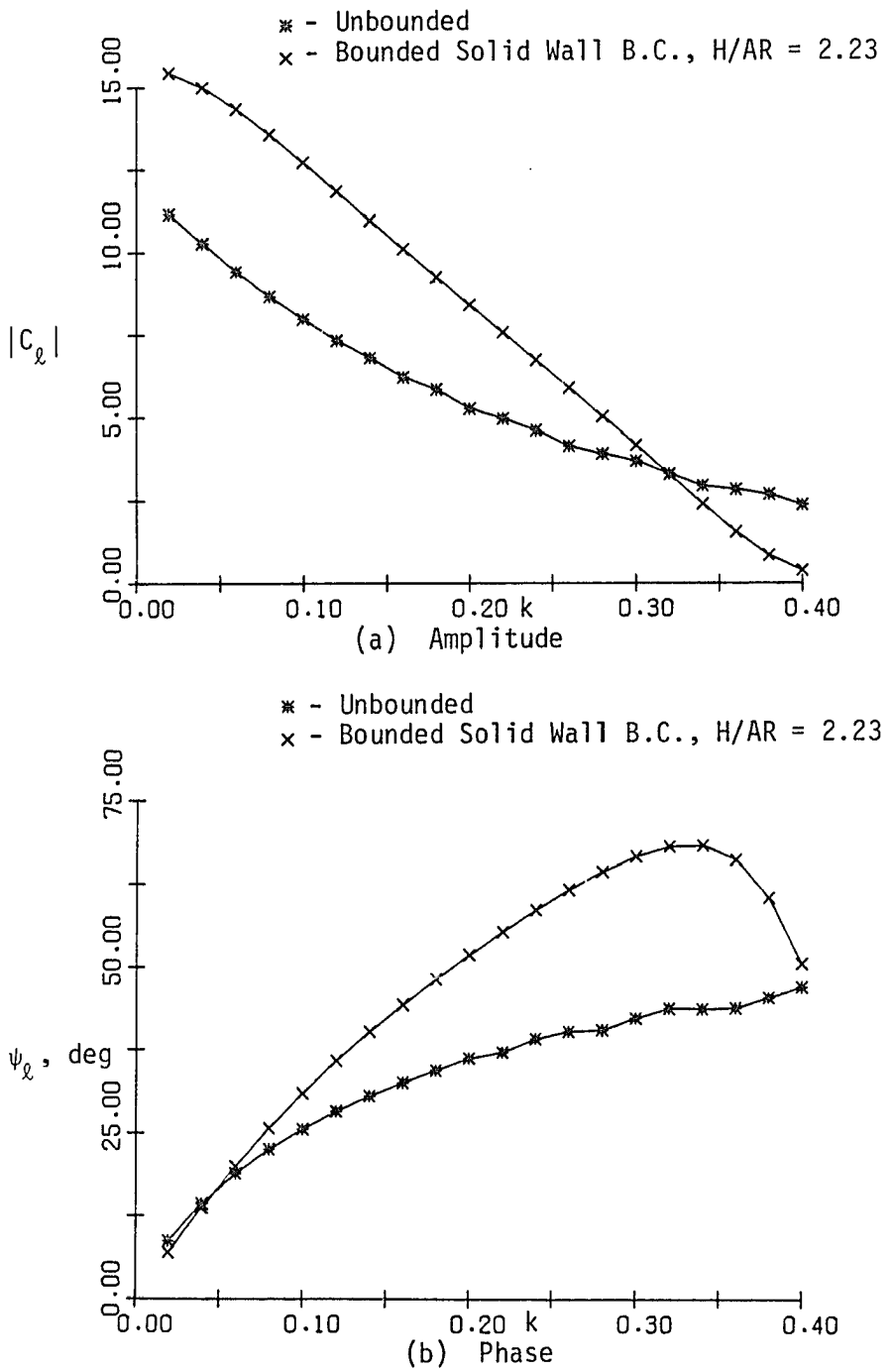

Figure 10. Lift coefficients vs. reduced frequency for a pitching NACA 64A010 rectangular wing, $M_\infty = 0.8$, AR = 3.8, $C_\ell = \alpha_1 |C_\ell| \sin(\omega t - \psi_\ell)$, solid wall boundary conditions.

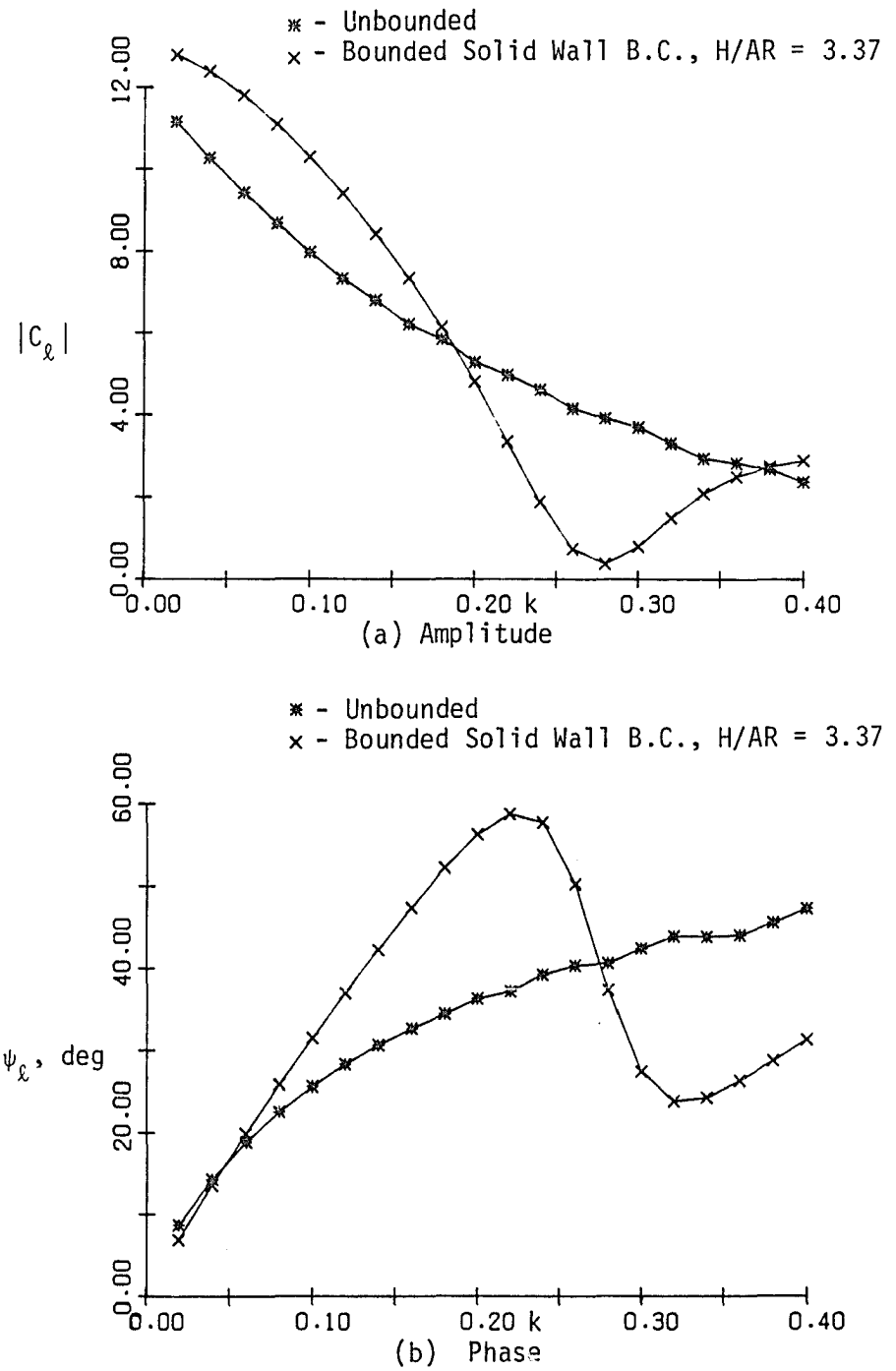

Figure 11. Lift coefficients vs. reduced frequency for a pitching NACA 64A010 rectangular wing, $M_\infty = 0.8$, AR = 3.8, $C_\ell = \alpha_1 |C_\ell| \sin(\omega t - \psi_\ell)$, solid wall boundary conditions.

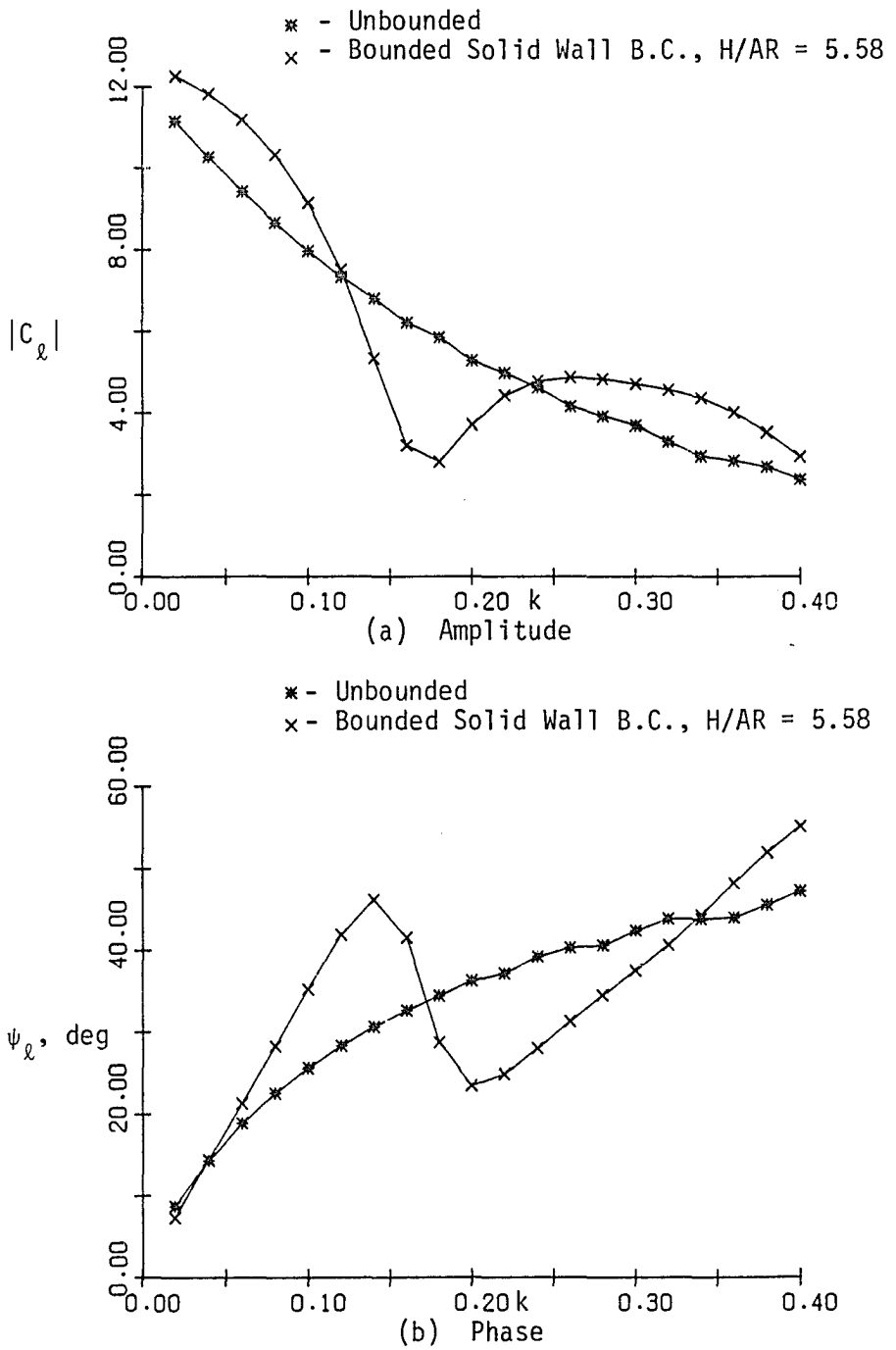

Figure 12. Lift coefficients vs. reduced frequency for a pitching NACA 64A010 rectantular wing, M_∞ = 0.8, AR = 3.8, C_ℓ = $\alpha_1 |C_\ell| \sin(\omega t - \psi_\ell)$, solid wall boundary conditions.

smaller. This is in accord with our two-dimensional observations. We observed that the three-dimensional resonant frequency is shefted towards higher frequencies in comparison with the two-dimensional results. It seems likely that there are additional resonant frequencies of higher values of k than those considered here.

The last experiment is for a square wind tunnel with a height of 12.8 chord lengths and the asymptotic boundary conditions given by equation (3.1). A comparison of the unbounded flow calculations with the bounded ones is shown in Figure 13. We note that three-dimensional bounded flow qualitatively agrees with the two-dimensional one, but differences between results for unbounded flow and those for bounded flow show that the effects are comparable, but smaller, in the three simensions than in two dimensions. Thus, as expected, unsteady wall interference in three-dimensional flow is somewhat less severe than that in two-dimensional cases. Nevertheless, it surely compromises many investigations.

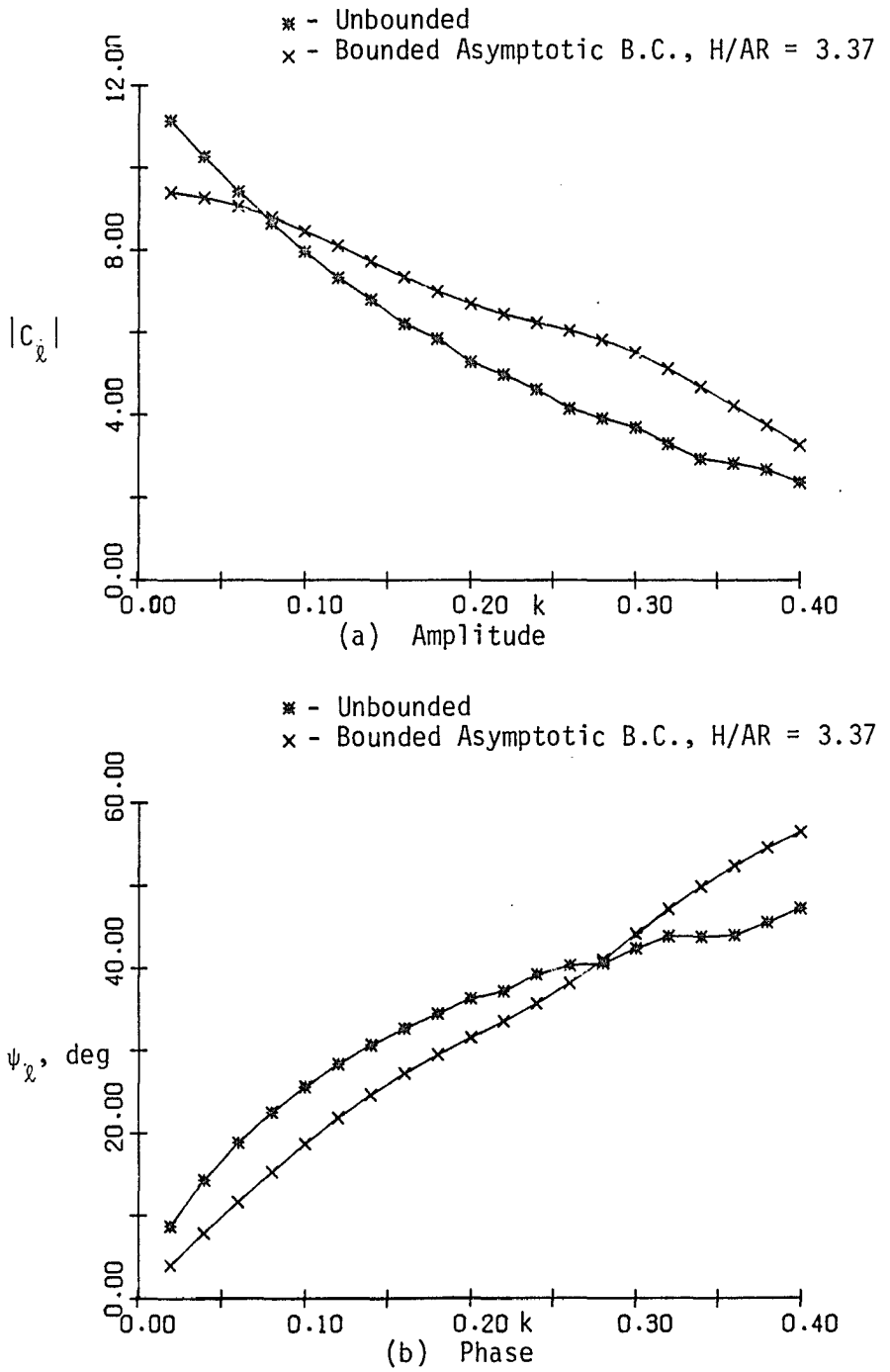

Figure 13. Lift coefficients vs. reduced frequency for a pitching NACA 64A010 rectangular wing, $M_\infty = 0.8$, AR = 3.8, $C_\ell = \alpha_1 |C_\ell| \sin(\omega t - \psi_\ell)$, asymptotic boundary conditions.

Chapter 5

CONCLUSIONS

The effects of wall interference on unsteady transonic flows were studied by imposing various numerical boundary conditions in order to simulate wind tunnel walls. We are able to show that the main discrepancy in the low frequency range ($k \lesssim 0.2$) between unconfined computations and confined experiments is due to nonlinear effects. At the higher reduced frequencies linear waves are reflected from the wind tunnel wall, causing serious discrepancies in the measured phase lags.

Although various techniques can be used in steady wind tunnel testing to minimize wall reflections, we have shown that wind tunnel wall effects remain in unsteady wind tunnel testing even they they have been essentially eliminated in the steady flow. This can occur even when the walls are ten chord lengths or more from the airfoil or wing being tested. Thus, wind tunnel walls can have a substantial effect on measured unsteady aerodynamic responses and such results must be viewed with suspicion until we are able to design wind tunnels that mitigate or eliminate wall reflections or until further numerical studies allow us to correct these measurements for wall reflections. This is probably only possible with solid walls. Wall interference is, of course, most important under resonant conditions, and resonances are shown to occur even in these nonlinear flows for reduced frequencies of practical interest.

A comparison of two-dimensional and three-dimensional results shows that wind tunnel wall interference in three dimensions, while smaller, is comparable to that in two dimensions. Our numerical experiments also show that a slotted tunnel does, to some extent, absorb incoming linear waves of low frequency and thereby reduce wall interference to acceptable levels for $k \lesssim 0.2$.

Experience with the codes based on a parabolic ADI schems shows that a numerical instability arises when the time step is not small enough (typically 360 time steps per cycle of motion are required). It would be of interest to solve the governing equation by an ADI split designed for hyperbolic equations, such as the D'Yakonov scheme, since the governing equation is hyperbolic.

REFERENCES

Bailey, F.R. and Steger, J.L., 1973. "Relaxation Techniques for Three-Dimensional Transonic Flow about Wings," AIAA Journal, Vol. 11, pp. 318-325.

Ballhaus, W.F. and Goorjian, P.M., 1978. "Computation of Unsteady Transonic Flows by the Indicial Method," AIAA Journal, Vol. 16, pp. 117-124.

Bliss, D.B., 1982. "Aerodynamic Behavior of a Slender Slot in a Wind Tunnel Wall," AIAA Journal, Vol. 20, pp. 1244-1252.

Borland, C., Rizzetta, D. and Yoshihara, H., 1980. "Numerical Solution of Three-Dimensional Unsteady Transonic Flow over Swept Wings," AIAA-80-1369, AIAA 13th Fluid and Plasma Dynamics Conference, Snowmass, Colorado.

Davis, S.S. and Malcolm, G.N., 1980. "Experimental Unsteady Aerodynamics of Conventional and Supercrital Airfoils," NASA TM-81221.

Douglas, J. and Rachford, H.H., 1956. "On the Numerical Solution of Heat Conduction Problems in Two and Three Space Variables," Transactions of the American Mathematical Society, Vol. 82, pp. 421-439.

Engquist, B. and Majda, A., 1981. "Numerical Radiation Boundary Conditions for Unsteady Transonic Flows," Journal of Computational Physics, Vol. 40, pp. 91-103.

Engquist, B. and Osher, S., 1980. "Stable and Entropy Satisfying Approximations for Transonic Flow Calculations," Mathematics of Computations, Vol. 34, pp. 45-75.

Ferri, A. and Baronti, P., 1973. "A Method for Transonic Wind Tunnel Corrections," AIAA Journal, Vol. 11, pp. 63-66.

Fung, K.-Y., 1981. "Far Field Boundary Conditions for Unsteady Transonic Flows," AIAA Journal, Vol. 19, pp. 180-183.

Fung, K.-Y. and Chung, A., 1982. "Computation of Unsteady Transonic Aerodynamic Responses Using a Prescribed Input Steady State Pressure Distribution," AIAA-82-0956, AIAA/ASME 3rd Joint Thermophysics, Fluids, Plasma and Heat Transfer Conference, St. Louis, Missouri.

Fung, K.-Y., Yu, N.J. and Seebass, A.R., 1978. "Small Unsteady Perturbations in Transonic Flows," AIAA Journal, Vol. 16, pp. 815-822.

Goodyer, M.J., 1975. "Self-Streaming Wind Tunnel," NASA TMX-72699.

Goorjian, P.M. and Van Buskirk, R., 1981. "Implicit Calculations of Transonic Flows Using Monotone Methods," AIAA 19th Aerospace Sciences Meeting, St. Louis, Missouri.

Hessenius, K.A. and Goorjian, P.M., 1982. "Validation of LTRAN2-HI by Comparison with Unsteady Transonic Experiment," AIAA Journal, Vol. 20, pp. 731-732.

Houwink, R. and van der Jooren, J., 1980. "Improved Version of LTRAN2 for Unsteady Transonic Flow Computations," AIAA Journal, Vol. 18, pp. 1008-1010.

Jameson, A., 1978. "Transonic Flow Calculations," Numerical Methods in Fluid Dynamics, A von Karman Institute Book, Edited by Wirz, H.J. and Smoldern, J.J., pp. 1-87.

Landahl, M.T., 1961. "Unsteady Transonic Flow," Pergamon Press, New York.

Lin, C.C., Reissner, E. and Tsien, H.S., 1948. "On Two-Dimensional Non-Steady Motion of a Slender Body in Compressible Fluid," Journal of Mathematics and Physics, Vol. 3, pp. 220-231.

Mitchell, A.R., 1976. "Computational Methods in Partial Differential Equations," John Wiley and Sons, London, pp. 220-223.

Murman, E.M. and Cole, J.D., 1971. "Calculations of Plane Steady Transonic Flow," AIAA Journal, Vol. 9, pp. 114-121.

Przybytkowski, S.M., 1983. "An Algorithm for Three-Dimensional Unsteady Transonic Flows," Engineering Experiment Station, College of Engineering, The University of Arizona, Report TFD 83-01.

Sears, W.R., 1977. "A Note on Adaptive-Wall Wind Tunnels," Journal of Applied Mathematics and Physics (ZAMP), Vol. 28, pp. 915-927.

Tijdeman, H. and Seebass, A.R., 1980. "Transonic Flow Past Oscillating Airfoils," Annual Review of Fluid Mechanics, Vol. 20, pp. 181-222.

Woolston, D.S. and Runyan, H.L., 1955. "Some Considerations on the Air Forces on a Wing Oscillating Between Two Walls for Subsonic Compressible Flow," Journal of the Aeronautical Sciences, pp. 41-50.